© 2015. Published by The Company of Biologists Ltd | Development (2015) 142, 1971-1977 doi:10.1242/dev.119404

RESEARCH REPORT

Diversity of epithelial morphogenesis during eggshell formation in drosophilids

Miriam Osterfield[1,*], Trudi Schüpbach[2], Eric Wieschaus[2] and Stanislav Y. Shvartsman[1,3]

ABSTRACT

The eggshells of drosophilid species provide a powerful model for studying the origins of morphological diversity. The dorsal appendages, or respiratory filaments, of these eggshells display a remarkable interspecies variation in number and shape, and the epithelial patterning underlying the formation of these structures is an area of active research. To extend the analysis of dorsal appendage formation to include morphogenesis, we developed an improved 3D image reconstruction approach. This approach revealed considerable interspecies variation in the cell shape changes and neighbor exchanges underlying appendage formation. Specifically, although the appendage floor in *Drosophila melanogaster* is formed through spatially ordered neighbor exchanges, the same structure in *Scaptodrosophila pattersoni* is formed through extreme changes in cell shape, whereas *Drosophila funebris* appears to display a combination of both cellular mechanisms. Furthermore, localization patterns of Par3/Bazooka suggest a self-organized, cell polarity-based origin for the variability of appendage number in *S. pattersoni*. Our results suggest that species deploy different combinations of apically and basally driven mechanisms to convert a two-dimensional primordium into a three-dimensional structure, and provide new directions for exploring the molecular origins of interspecies morphological variation.

KEY WORDS: Epithelial morphogenesis, Tube formation, Evolution, *Drosophila*, *Scaptodrosophila*

INTRODUCTION

The extent of morphological diversity across the animal kingdom is extremely large, but our current understanding of how this diversity arises is limited (Mallarino and Abzhanov, 2012). One promising system for studying evolution and morphogenesis is the drosophilid eggshell. In all species of the Drosophilidae family, the anterior region of each eggshell contains several specialized structures, the most prominent of which are the dorsal appendages, which are also called the respiratory filaments. Eggshell components are produced by the follicle cells, which cover the developing oocyte (Fig. 1A). The follicle cells secrete these components into the space between their apical surfaces and the oocyte. Therefore, the shape of the eggshell reflects the final morphology of the follicular epithelium. The dorsal appendages are therefore the products of epithelial tubes, formed by cell rearrangements, cell shape changes and cell migration (Dorman et al., 2004).

[1]Lewis-Sigler Institute for Integrative Genomics, Princeton University, Princeton, NJ 08544, USA. [2]Department of Molecular Biology, Princeton University, Princeton, NJ 08544, USA. [3]Department of Chemical and Biological Engineering, Princeton University, Princeton, NJ 08544, USA.

*Author for correspondence (mosterfi@princeton.edu)

Received 3 November 2014; Accepted 30 March 2015

The dorsal appendages display striking interspecies variation in number and shape (Hinton, 1981); so far, attempts to explain this variation have focused on patterning of the follicular epithelium. The control of dorsal appendage formation in *D. melanogaster* eggshells has been extensively studied, with a major focus on patterning by morphogen gradients and the downstream cascades of signaling and transcription (Berg, 2005; Cheung et al., 2011; Wu et al., 2008). Several studies have also examined patterning of the follicular epithelium in other drosophilid species (James and Berg, 2003; Kagesawa et al., 2008; Marmion et al., 2013; Nakamura et al., 2007; Nakamura and Matsuno, 2003; Niepielko et al., 2011, 2012, 2014; Niepielko and Yakoby, 2014; Peri et al., 1999; Vreede et al., 2013; Zartman et al., 2008). However, the mechanisms responsible for the observed differences in shapes and number of respiratory filaments are still unclear.

In *D. melanogaster*, where eggshell patterning and morphogenesis have been studied most extensively, the first phase of tube morphogenesis appears to be driven by apical patterns of forces that cause cell neighbor rearrangements and tissue buckling (Osterfield et al., 2013). Subsequent tube elongation, by contrast, appears to be driven basally; specifically, the basal sides of the appendage-forming cells crawl forward on the surrounding extracellular matrix, pulling the apical surface into an elongated shape (Boyle and Berg, 2009; French et al., 2003; Peters et al., 2013). This raises the question: which, if any, of these morphogenetic mechanisms are conserved in other species? Here, we use a 3D image reconstruction approach to address this question in species with clear differences in the number and shape of dorsal appendages.

RESULTS AND DISCUSSION

In this study, we compare similarities and difference in morphogenesis among *D. melanogaster*, *Drosophila funebris* and *Scaptodrosophila pattersoni*, the eggshells of which are shown in Fig. 1B. While the *D. melanogaster* egg invariably has two appendages with larger paddle structures at the end, *D. funebris* eggs have four appendages and *S. pattersoni* eggs have a variable number of long thin appendages.

As described in previous work (Osterfield et al., 2013), we believe that appendage formation in *D. melanogaster* can be understood to a significant degree by considering just the apical surface of the follicular epithelium. With this in mind, we set out to reconstruct apical surfaces of the follicular epithelium in additional species. The apical surface can be described essentially as a two-dimensional (2D) network of vertices and cell-cell edges embedded in 3D space. To visualize this network, we took confocal *z*-stack images in which an adherens junction marker, either E-cadherin or β-catenin, was fluorescently labeled. We then adapted algorithms developed to trace neurites and other filamentous structures (Haas-Koffler et al., 2012; Meijering et al., 2004) to reconstruct the network of apical edges in our data, using the existing image-tracing software as a computer-guided '3D camera lucida'.

Development (2015) 142, 1971-1977 doi:10.1242/dev.119404

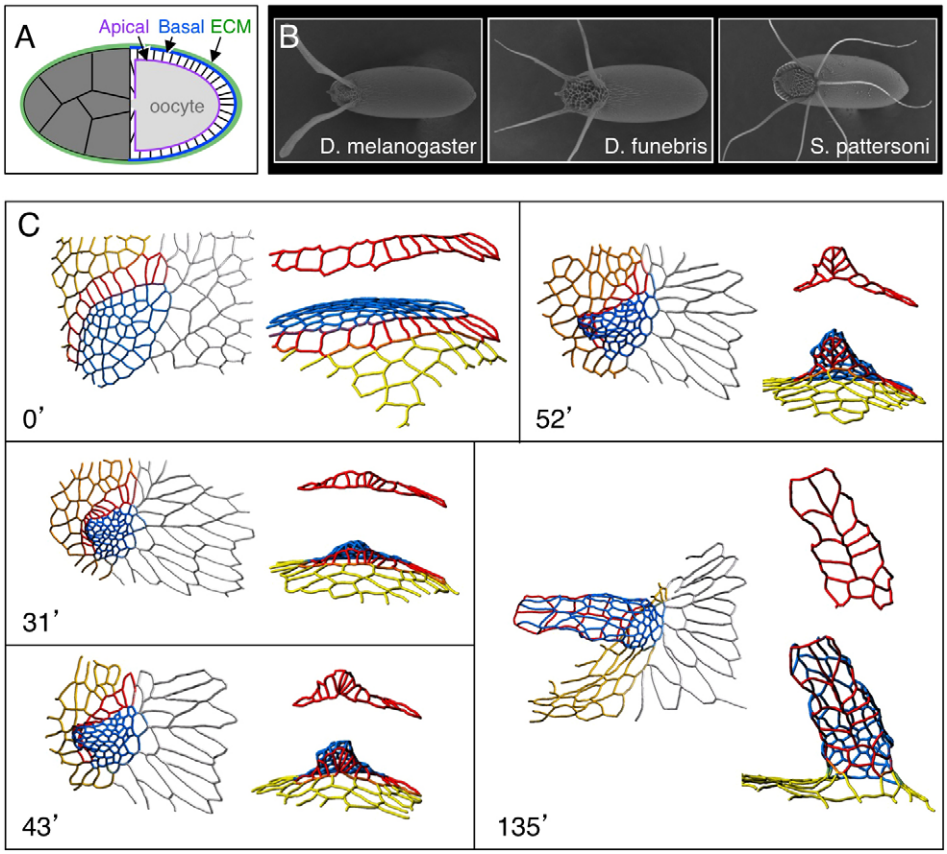

Fig. 1. Drosophilid eggs provide a useful system for studying changes in morphogenesis across related species. (A) Schematic of a developing egg chamber shortly before the onset of dorsal appendage formation. The oocyte (light gray) is surrounded by a monolayer of follicle cells, the apical surfaces (purple) of which face inwards toward the oocyte and the basal surfaces (blue) of which face outwards towards the basement membrane or extracellular matrix (ECM; green). The nurse cells (dark gray), which make up the rest of the egg chamber, are not specifically examined in this study. (B) Scanning electron microscope (SEM) images of eggshells from the species considered in this paper. These eggs differ in both number and shape of dorsal appendages. (C) 3D reconstructions of dorsal appendage formation in *D. melanogaster*. The filament-tracing module of Imaris was used to trace the apical outlines of follicle cells, visualized with E-cadherin:GFP. The primary data, a time-lapse confocal *z* series, has been described in a previous publication (Osterfield et al., 2013). Times from the beginning of the movie, rounded to the nearest minute, are indicated in each box. Putative cell types were assigned according to cell morphology and color-coded as follows: blue, roof; red, floor; yellow, 'midline' or operculum-forming cells; gray, main body cells. Dorsal views are shown in the left of each box. Views chosen to optimize visualization of the floor cells (roughly, from the dorsal-anterior) are shown on the right, including either floor cells only (above) or roof+floor+midline (below).

D. melanogaster: tube formation through ordered floor cell intercalation

As a first test of this approach, we performed 3D reconstructions of several time points from a previously characterized time-lapse movie (Osterfield et al., 2013). This movie captures the early phase of dorsal appendage formation in a *D. melanagaster* egg chamber that expresses E-cadherin:GFP. To aid visualization, we have color-coded the edges in our reconstructions according to presumptive cell type, using cell morphology as a guide. The tissue shape changes and cell neighbor rearrangements involved in dorsal appendage tube formation are clearly visible in these 3D image reconstructions (Fig. 1C; supplementary material Movie 1). Of particular note are the roof (blue) and floor (red) cell types that form the roof and floor, respectively, of the final appendage structure (Dorman et al., 2004). The tissue shape changes and cell neighbor rearrangements involved in dorsal appendage tube formation are clearly visible in these 3D image reconstructions (Fig. 1C). Most informative are the changes in the floor cell domain, shown in red. Before the onset of appendage formation, the floor domain is a one-cell wide row of cells separating the roof cells (blue) from the so-called 'midline' or operculum-forming cells (yellow) within a relatively flat sheet. As the appendage forms, this domain converts into a two-cell wide row of cells that forms the floor of a highly curved tube. This transformation occurs, at least in part, as a result of floor cells exchanging contacts with operculum-forming cells for new contacts with other floor cells, through a spatially ordered sequence of cell rearrangements (Osterfield et al., 2013).

S. pattersoni: tube formation with major floor cell shape changes

Having validated our image reconstruction approach in *D. melanogaster*, we went on to analyze eggshell morphogenesis in *S. pattersoni*, a member of the *Scaptodrosophila* genus, in which eggs generally have a large and variable number of filaments. Using β-catenin immunostaining to visualize apical edges, we reconstructed 3D networks from a series of fixed time points (Fig. 2A-D). Strikingly, this analysis revealed that all of the filaments in an egg chamber develop from a single primordium.

During *S. pattersoni* appendage formation, the first cell types to become visually distinct are the midline and floor cell types, which exhibit increased levels of β-catenin (Fig. 2A,A′). The roof domain then becomes recognizable by a smoothened posterior border and a significant reduction in apical cell area (Fig. 2B). As the tubes form, the roof cells rearrange contacts among themselves to transition from a domain with a single concave border on its anterior side, to a domain

Development (2015) 142, 1971-1977 doi:10.1242/dev.119404

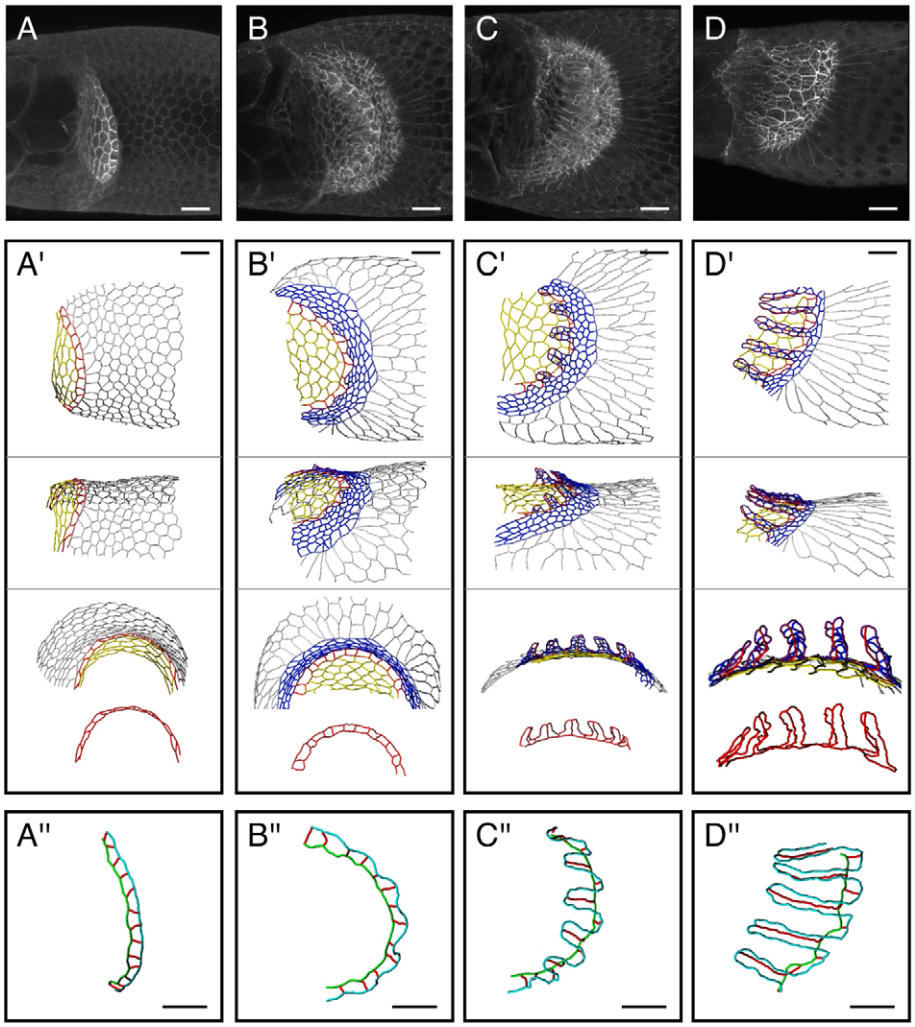

Fig. 2. *S. pattersoni* tube formation occurs with major changes in floor cell shape, but little or no cell rearrangement along the floor-operculum boundary. (A-D) *S. pattersoni* egg chambers, immunostained for β-catenin, arranged by increasing developmental stage. Representative samples were chosen for tracing from among 92 samples ranging from late stage 10B through stage 12. Dorsal or dorsolateral view. Anterior is leftwards. (A′-D′) 3D reconstructions of data from A-D. Putative cell types were assigned according to cell morphology and color-coded: blue, roof; red, floor; yellow, 'midline' or operculum-forming cells; gray, main body cells. Views shown are approximately dorsal (top panel), lateral (middle) and anterior (bottom). (A″-D″) 3D reconstructions of the floor cells only. The floor-midline (or floor-operculum) boundary (green) appears to undergo little morphological change. By contrast, the floor-roof boundary (cyan) becomes greatly elongated, while it simultaneously gains contacts with increasing numbers of roof cells (see A′-D′). Floor-floor edges (red) either grow greatly in length and extend anteriorly, or retain roughly their original size and position; these two outcomes alternate spatially, resulting in a series of tubes with two floor cells each. Scale bars: 20 µm.

with several finger-like anterior protrusions, creating roofs for each of the tubes as they form (Fig. 2A′-D′; supplementary material Movie 2). Although roof domain behavior looks different between *D. melanogaster* and *S. pattersoni* at the level of gross morphology, it seems likely that the underlying behaviors of roof cells are similar. In particular, cell neighbor rearrangements among the roof cells are consistent with an accommodation to mechanical stresses imposed by a lengthening floor-roof boundary (cyan traces in Fig. 2A″-D″).

By contrast, the floor cells in *S. pattersoni* behave in a fundamentally different way from their counterparts in *D. melanogaster* (Fig. 2A″-D″). Most notably, the single row of floor cells does not appear to form new floor-floor edges through rearrangements along the floor-midline border (green traces in Fig. 2A″-D″), because throughout morphogenesis each floor cell contacts at most two other floor cells, one to the right and one to the left (red traces in Fig. 2A″-D″). Instead, the floor cells undergo a dramatic change in cell shape. Alternating floor-floor edges greatly lengthen, extending all the way to the tip of the appendage, while the remaining set of floor-floor edges largely retain their original position and length. In other words, no new floor-floor edges are formed, and the 'seam' running along the bottom of each tube is actually formed from an existing floor-floor edge that has simply become extremely long.

It appears unlikely that the forces and cell properties associated with a particular cell type (i.e. roof or floor) are strictly conserved between *D. melanogaster* and *S. pattersoni*. This is made particularly clear by considering the eggs of *D. melanogaster* with hypomorphic Ras mutations. The egg chambers of these patterning mutants have a single primordium in which floor and roof cells are initially found in a similar geometrical arrangement to *S. pattersoni*, but the eggshells have only a single appendage (Ward and Berg, 2005).

What might our observations suggest about alternative mechanisms driving dorsal appendage morphogenesis in *S. pattersoni*? Furthermore, do these observations yield any insight into how a variable number of appendages – even among eggshells from the same mother (Fig. 3A-F) – can be generated from a single primordium?

The shape changes in the floor cells are likely to be driven by forces external to the floor cells themselves, as cell-autonomously driven apical expansion and extension along one axis is hard to explain mechanically and has no precedent, to our knowledge. One obvious source for the force driving floor cell elongation could come from the basal surfaces of the follicle cells crawling along the overlying basement membrane. This pulling force would then be transmitted to the apical edges through the lateral surfaces of the cells. In other words, we suggest that the mechanism promoting elongation of filaments in one species (*D. melanogaster*) may be deployed earlier in another species (*S. pattersoni*) to initiate filament formation. This is further supported by the tilted 3D shape of the midline and floor cells, in which apical surfaces trail behind the anteriorly advancing basal surface (data not shown).

If tube formation is indeed driven by basal pulling, how could this result in the formation of multiple tubes? One possibility is that the pulling force is only applied to alternating floor-roof vertices or

Development (2015) 142, 1971-1977 doi:10.1242/dev.119404

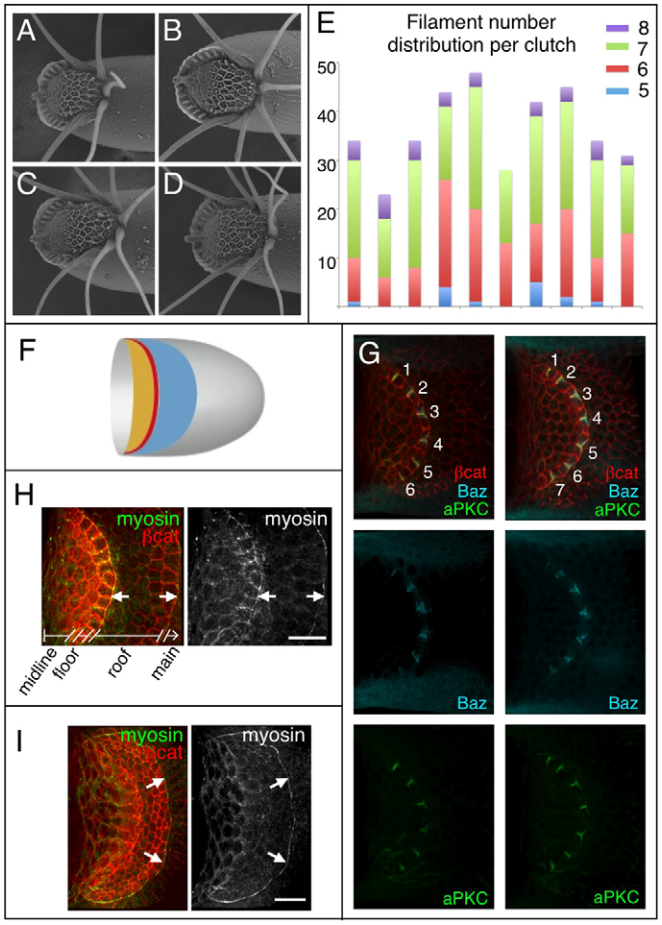

Fig. 3. *S. pattersoni* eggs have a variable number of dorsal appendages that all arise from a single primordium. (A-D) SEM images of *S. pattersoni* eggshells, with 5, 6, 7 or 8 dorsal appendages. (E) To examine the distribution of appendage number in eggs from a single clutch, gravid females were dissected, and those with fully developed (stage 14) eggs were analyzed. The distribution of appendage number in eggs from each female is represented by a single stacked bar. Averaging across the ten clutches examined, the appendage number distribution is: 5, 4%; 6, 36%; 7, 51.5%; 8, 8.5%. (F) Proposed spatial pattern of follicle cell types in *S. pattersoni*, dorsal view, with color-coding: blue, roof; red, floor; yellow, 'midline' or operculum-forming cells; gray, main body cells. This fate map is based on the data in H and in Fig. 2. (G) Immunostaining of *S. pattersoni* egg chambers for β-catenin (red), Bazooka (cyan) and aPKC (green). Images were cropped to remove the basal surface and reveal the underlying apical surface. (H,I) Immunostaining of *S. pattersoni* egg chambers for β-catenin (red) and phospho-myosin regulatory light chain (green). Phospho-myosin regulatory light chain is also shown alone in the right-hand panels. Images were cropped to remove the basal surface and reveal the underlying apical surface. (H) At early stages before significant roof cell constriction, myosin cables (arrows) border the single roof domain both to the anterior and posterior. (I) At later stages with constricted roof cells, myosin accumulates apically throughout the appendage-forming region, while the myosin cable along the roof-main body border also remains prominent. Anterior is leftwards. Scale bars: 20 µm.

floor-floor edges. Alternatively, these may experience equal forces, while the relative deformability of the floor-floor edges alternates. To explore these possibilities, we examined the localization of myosin and the polarity protein Par3/Bazooka, as spatial patterning of these molecules within the apical surface of follicle cells was previously proposed to drive appendage morphogenesis in *D. melanogaster* (Osterfield et al., 2013).

In *S. pattersoni*, we found that Bazooka localizes specifically to alternating floor-floor edges (Fig. 3G), in particular to the subset of edges that lengthen and subsequently form the bottom of each appendage tube (supplementary material Movie 3). These edges also exhibit staining for atypical Protein Kinase C (aPKC), which colocalizes and functions with Par3/Bazooka in several different types of cell polarization events (Suzuki and Ohno, 2006). The number of edges that are positive for Bazooka and aPKC varies among egg chambers; out of 10 examined samples of stages similar to Fig. 3G, seven samples had six edges that were positive for Baz and aPKC, whereas three had seven such edges. This correlates relatively well with the variability we found in eggshell type, with seven and six appendages being the most common (Fig. 3E). These results suggest that some type of self-organized mechanism for patterning cell polarity could underlie the variability in appendage number. The exact mechanism that determines appendage number, e.g. through the number of floor cells specified or some feature of the system propagating polarity information, remains an interesting but unresolved issue.

Surprisingly, myosin localization at this stage did not appear to be complementary to Bazooka, unlike in *D. melanogaster* follicle cells during dorsal appendage formation (Osterfield et al., 2013) or embryos during germband extension (Bertet et al., 2004; Zallen and Wieschaus, 2004). Instead, the roof domain is bounded on both the anterior and posterior sides by myosin cables as the appendage primordium first becomes morphologically apparent (Fig. 3H), and at later times when the floor domain begins to buckle, apical localization throughout the appendage forming region is fairly diffuse, with the only prominent myosin-enriched feature being the posterior cable that separates roof from main body cells (Fig. 3I). However, it remains possible that myosin localization to specific floor-floor edges occurs, but is too weak or transient for our detection methods. The lack of clear myosin localization to specific floor-floor edges leaves us without an obvious mechanism for generating differences in mechanical properties between the two classes of floor-floor edges. However, the recruitment of Bazooka and aPKC specifically to the lengthening edges demonstrates that these morphologically distinct classes of edges are also molecularly distinct. It will be interesting in the future to further characterize differences in molecular composition between these classes of edges and to examine the consequences of these differences for membrane trafficking, tension or other physical properties.

D. funebris: combined cell shape changes and neighbor exchange

Filament morphogenesis appears surprisingly different in *S. pattersoni* compared with *D. melanogaster*, so we next set out to examine morphogenesis in a more closely related species; for this purpose, we chose *D. funebris* (Russo et al., 1995). First, we examined the initial shape of appendage primordia by immunostaining for the transcription factor Broad, a well-established marker for roof cell fate (Dorman et al., 2004). Although *D. funebris* eggs have four appendages, the egg chambers contain only two Broad expression patches. Each of the Broad-positive primordia is kidney bean shaped; i.e. the anterior border is not entirely convex, as in *D. melanogaster*, but is concave in the middle with two flanking convex regions (Fig. 4A,B). This shape is also apparent in samples immunostained for β-catenin as a region of cells with reduced apical area surrounded by a smoothened border (Fig. 4C,D). Two similarly shaped primordia have previously been described in *D. virilis* (James and Berg, 2003), another member of the *Drosophila* subgenus with four appendages. This similarity is consistent with previous suggestions that the shape of the primordium helps determine appendage number in some cases (Zartman et al., 2011).

Development (2015) 142, 1971-1977 doi:10.1242/dev.119404

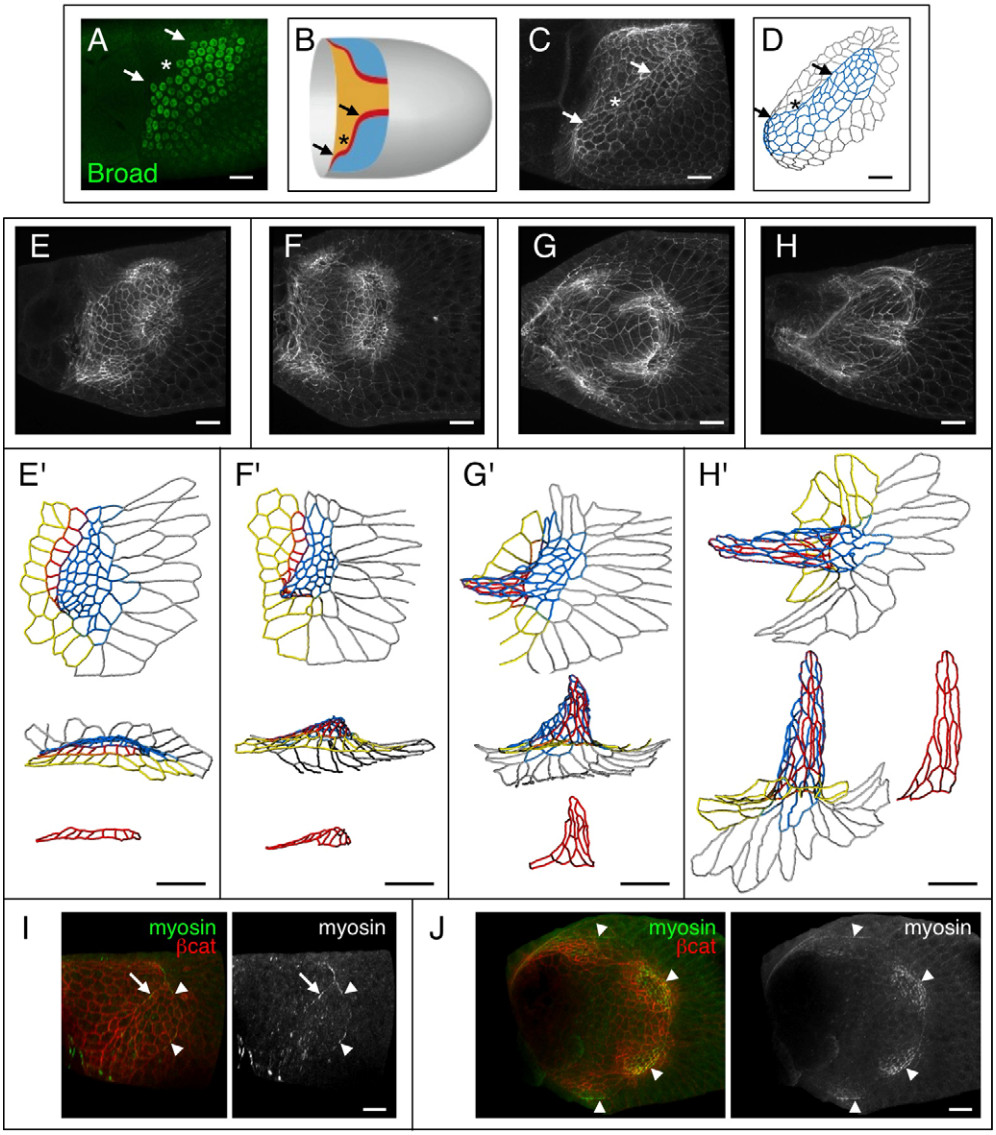

Fig. 4. *D. funebris* tube formation involves changes in both floor cell shape and the floor-operculum boundary. (A) *D. funebris* egg chamber immunostained for Broad, a marker for roof cells. Lateral view, anterior is leftwards. Convex (arrows) and concave (asterisk) regions of anterior roof boundary are indicated in A-D. (B) Proposed spatial pattern of follicle cell types in *D. funebris*, using Broad staining (A) as a guide. Color-coding as in Fig. 1C. Dorsal view. (C) *D. funebris* egg chamber of similar stage to A, immunostained for β-catenin. Lateral view, anterior is leftwards. (D) 3D reconstruction of data from C. The early appendage primordium is morphologically apparent as a domain of apically constricted cells with a smooth boundary. These cells are colored blue here, to indicate proposed roof cell identity. (E-H) *D. funebris* egg chambers immunostained for β-catenin, arranged by increasing developmental stage. Representative samples were chosen for analysis from among 25 samples ranging from late stage 10B through stage 12. Dorsolateral (E,H) or dorsal (F,G) views; anterior towards the left. (E′-H′) 3D reconstructions from E-H, showing only the lower-posterior appendage. Color-coding: blue, roof; red, floor; yellow, 'midline' or operculum-forming cells; gray, main body cells. Upper figures are from same point of view as E-H. Views chosen to optimize visualization of the floor cells (roughly, from the anterior) are shown below, including either floor cells only or all four cell types. (I,J) Immunostaining of *D. funebris* egg chambers for β-catenin (red) and phospho-myosin regulatory light chain (green). Phospho-myosin regulatory light chain is also shown alone in the right-hand panels. Images were cropped to remove the basal surface and reveal the underlying apical surface. (I) At early stages, myosin cables can be seen on the anterior (arrow) and posterior (arrowheads) border of the roof domain. Lateral view, anterior is leftwards. (J) At later stages when 3D rearrangements begin, myosin accumulates apically through the appendage-forming region and remains localized to the roof-main body border (arrowheads), but a myosin cable on the floor-midline border is not apparent. Dorsal view, anterior is leftwards. Scale bars: 20 µm.

Our 3D reconstruction of epithelial morphogenesis in *D. funebris* revealed the following sequence of events. Each primordium develops into two distinct, buckled patches of highly constricted cells (Fig. 4E). Each of these two buckled regions then elongates (Fig. 4F-H), resulting in the eventual formation of four tubes per egg chamber. To study how a single buckled domain is transformed into a tube in this species, we focused on the more posterior tubes (Fig. 4E′-H′, supplementary material Movie 4), which can be relatively easily compared with the appendages in *D. melanogaster*, due to similarities in shape, position and cell number. Our examination of the floor cell domain reveals that *D. funebris* has both similarities and differences with the two species discussed above. Several of the floor cells lengthen significantly, reminiscent of *S. pattersoni*, but unlike in that species, the floor-midline boundary of *D. funebris* appears to undergo rearrangements resulting in increased numbers of floor-floor boundaries. Although these cell neighbor

Development (2015) 142, 1971-1977 doi:10.1242/dev.119404

rearrangements clearly resemble those seen in *D. melanogaster*, they appear to be less ordered spatially: they initiate off-center (Fig. 4F′) and form a final floor domain with no clear seam or spatial structure (Fig. 4G′-H′). Furthermore, although myosin appears to be either recruited or activated apically throughout much of the appendage primordium, we do not observe a myosin cable on the floor-midline border (Fig. 4I,J). By contrast, our previous work suggested that a myosin cable along the floor-midline border is crucial for driving spatially ordered cell neighbor exchange in *D. melanogaster* (Osterfield et al., 2013). We therefore suggest that *D. funebris* appendage formation is not actively driven by ordered floor cell rearrangement. Instead, we hypothesize that pulling forces from the basal side provide the main driving force, with the floor domain passively yielding to this stress through a combination of cell shape changes and neighbor exchanges.

D. melanogaster: redundant morphogenetic mechanisms?

The results described above suggest that we should reconsider proposed mechanisms of dorsal appendage formation. In particular, a disordered appendage floor with no clear seam can be found not only in *D. funebris* (Fig. 4H′), but also in *D. melanogaster* patterning mutants, such as *fs(1)K10* (Ward and Berg, 2005) and CY2>Mae (supplementary material Fig. S1). Myosin does appear to form a cable along the floor-midline border in CY2>Mae (supplementary material Fig. S1E), but it is currently unclear whether this is sufficient to drive the pattern of cell rearrangements that occurs in this genetic background. Additionally, experiments from Celeste Berg and colleagues on the effect of ectopically expressing *rhomboid* in *D. melanogaster* follicle cells indicates that ectopic appendage tubes can form with as few as two cells, specifically one roof plus one floor (Ward and Berg, 2005). Cell neighbor rearrangements increasing the number of floor-floor edges are impossible in this case, raising the possibility that appendage formation in this genetic background may occur through a *pattersoni*-like mechanism involving changes in floor cell shape. Together, these observations highlight the need to dissect more carefully the relative contribution of myosin cable driven intercalation, basal pulling, roof cell constriction (Dorman et al., 2004) or other mechanisms as potential forces driving appendage formation in mutant and wild-type *D. melanogaster* egg chambers.

Conclusion

At the outset of this work, we expected that dorsal appendage formation in different species would occur through largely similar cellular mechanisms. In particular, we expected that appendage formation would be driven by ordered floor cell intercalations that were themselves driven by highly patterned apical tensions, as was observed in *D. melanogaster*. However, our studies of *S. pattersoni* provide a clear counter-example to this mechanism, revealing that tubes can form though changes in cell shape, rather than through neighbor exchanges within the floor domain. The inter-species variation in eggshell morphogenesis emphasizes a general point: the details of morphogenesis may be extremely important in understanding how changes in gene expression pattern lead to changes in morphology among evolutionarily homologous structures (Mallarino et al., 2012).

In spite of clear differences in cellular behavior during eggshell morphogenesis among the species we studied, it appears that different combinations of just a few physical mechanisms may be at work; testing these mechanisms in detail promises to be an interesting future direction. This study also helps lay the groundwork for future studies on the relationship between expression profiles and cellular properties in epithelial cells, and for studies exploring the degree to which mechanisms of epithelial morphogenesis are conserved across species.

MATERIALS AND METHODS

Fly stocks

D. melanogaster and *D. funebris* flies (*Drosophila* Species Stock Center, #15120-1911.01) were maintained on standard cornmeal media. To enrich for stage 11 egg chambers, yeast was added to the media 1 (*D. melanogaster*) or 2 (*D. funebris*) days before dissection. *S. pattersoni* flies (*Drosophila* Species Stock Center, #11010-0031.00) were generally maintained on standard cornmeal media supplemented with a small quantity (0.2-0.6 ml per vial) of banana purée (Gerber). To enrich for stage 11 egg chambers, *S. pattersoni* females and males were moved to cornmeal media within 1-2 days after eclosion, kept on cornmeal media for several days, then placed together on banana-supplemented media 1 day before dissection.

D. melanogaster genotypes used included E-cadherin:GFP transgenic flies for Fig. 1 (Huang et al., 2009), CY2-GAL4, UAS-Mae/CyO for supplementary material Fig. S1C,D and CY2-GAL4, UAS-Mae/ed [CPTI000616] for supplementary material Fig. S1A,B. The echinoid-YFP trap line ed[CPTI000616] was acquired from the DGRC in Kyoto, Japan. The CY2-GAL4, UAS-Mae/CyO line was a gift from J. Duffy (WPI, Worcester, MA, USA); the effect of this genotype on eggshell patterning has been described previously (Yamada et al., 2003).

Immunohistochemistry

Immunostaining was generally carried out as described previously (Osterfield et al., 2013; Ward and Berg, 2005). However, the protocol was modified for samples stained for phospho-myosin: after primary antibody incubation, samples were washed in 4°C with ice-cold PBSTwn for 3×10 min, post-fixed for 20 min at room temperature with 4% paraformaldehyde in PBSTwn, washed for 3×10 min and re-blocked in 1% bovine serum albumin (Sigma-Aldrich) in PBSTwn at least 1 hour before proceeding to the secondary antibody incubation step. For most samples, the final dilution series of glycerol/PBS was omitted. Instead, the samples were washed into RapiClear 1.47 (SunJin Lab, Taiwan) then mounted for imaging between two glass coverslips, which were separated by a 0.2 mm spacer (SunJin Lab, #IS007) and sealed with nail polish. Primary antibodies used included anti-β-catenin (anti-armadillo N2 7A1, mouse, Developmental Studies Hybridoma Bank, 1:20), anti-Broad-core (mouse, Developmental Studies Hybridoma Bank, 1:50), anti-Fasciclin III (7G10, mouse, Developmental Studies Hybridoma Bank, 1:50), anti-phospho-myosin light chain 2 (Ser 19) (rabbit, Cell Signaling Technology, 1:20), anti-Bazooka [guinea pig (Blankenship et al., 2006), 1:250-1:500] and anti-aPKC (rabbit, 1:1000, Santa Cruz Biotechnology). Atto 488-conjugated GFP-booster (1:200, ChromoTek) was used during the secondary antibody incubation step for enhancing echinoid-YFP signal. Alexa-Fluor-conjugated secondary antibodies (Invitrogen) were generally used at 1:500.

Microscopy and image processing

All fluorescent images were acquired using a Leica SP5 confocal microscope, with a 63× (NA 1.3) glycerol immersion objective. Images were adjusted for brightness/contrast and displayed as a maximum projection using either ImageJ/FIJI or the surpass mode of Imaris software (Bitplane). In several cases (Figs 3G-I and 4I,J; supplementary material Fig. S1E), images were cropped in 3D to remove the basal surface, which would otherwise block or overwhelm signal from the apical surface. Tracing of apical edges was carried out with the filament-tracing module of Imaris software, primarily using the AutoPath function, which allows for supervised automatic tracing (Meijering et al., 2004). The apical markers we used for tracing (E-cadherin or β-catenin) also localize to some extent to lateral surfaces, particularly in midline type cells, so direct proximity to the oocyte or appendage tube lumen was also considered in determining whether fluorescent signal indicated the presence of an apical edge. As all eggshells studied here appear to exhibit complete left-right symmetry, some images were flipped, either to preserve anterior=left and dorsal=up orientation, or (as

Development (2015) 142, 1971-1977 doi:10.1242/dev.119404

in Fig. 4) to allow easier comparison between structures that originally differed in left- versus right-handedness.

Acknowledgements

We thank Matthew Gastinger (Bitplane) for extensive guidance in using Imaris for 3D reconstructions; Nir Yakoby, Matt Niepielko, Rob Marmion, Anna DiPaola and Therese Markow for advice regarding fly species; Joe Goodhouse and Gary Laevsky for imaging advice; Jennifer Zallen for the generous gift of several anti-Bazooka antibodies; and Celeste Berg, Olivier Devergne and members of the Wieschaus, Schüpbach and Shvartsman labs for discussions. We also thank our three anonymous reviewers for helpful feedback and suggestions. Several stocks were obtained from the *Drosophila* Species Stock Center at the University of California, San Diego. Monoclonal antibodies originally developed by Gregory Guild, Eric Wieschaus and Corey Goodman were obtained from the Developmental Studies Hybridoma Bank, created by the NICHD of the NIH and maintained at The University of Iowa, Department of Biology, Iowa City, IA 52242.

Competing interests

The authors declare no competing or financial interests.

Author contributions

M.O. performed experiments and data analysis. M.O., T.S., E.W. and S.Y.S. developed the approach and prepared or edited the manuscript.

Funding

This research was funded by the National Institute of General Medical Sciences [1R01GM107103- 01A1]. E.W. is a HHMI Investigator. Deposited in PMC for release after 6 months.

Supplementary material

Supplementary material available online at
http://dev.biologists.org/lookup/suppl/doi:10.1242/dev.119404/-/DC1

References

Berg, C. A. (2005). The Drosophila shell game: patterning genes and morphological change. *Trends Genet.* **21**, 346-355.

Bertet, C., Sulak, L. and Lecuit, T. (2004). Myosin-dependent junction remodelling controls planar cell intercalation and axis elongation. *Nature* **429**, 667-671.

Blankenship, J. T., Backovic, S. T., Sanny, J. S. P., Weitz, O. and Zallen, J. A. (2006). Multicellular rosette formation links planar cell polarity to tissue morphogenesis. *Dev. Cell* **11**, 459-470.

Boyle, M. J. and Berg, C. A. (2009). Control in time and space: Tramtrack69 cooperates with Notch and Ecdysone to repress ectopic fate and shape changes during Drosophila egg chamber maturation. *Development* **136**, 4187-4197.

Cheung, L. S., Schüpbach, T. and Shvartsman, S. Y. (2011). Pattern formation by receptor tyrosine kinases: analysis of the Gurken gradient in Drosophila oogenesis. *Curr. Opin. Genet. Dev.* **21**, 719-725.

Dorman, J. B., James, K. E., Fraser, S. E., Kiehart, D. P. and Berg, C. A. (2004). bullwinkle is required for epithelial morphogenesis during Drosophila oogenesis. *Dev. Biol.* **267**, 320-341.

French, R. L., Cosand, K. A. and Berg, C. A. (2003). The Drosophila female sterile mutation twin peaks is a novel allele of tramtrack and reveals a requirement for TTK69 in epithelial morphogenesis. *Dev. Biol.* **253**, 18-35.

Haas-Koffler, C. L., Naeemuddin, M. and Bartlett, S. E. (2012). An analytical tool that quantifies cellular morphology changes from three-dimensional fluorescence images. *J. Vis. Exp.* e4233.

Hinton, H. E. (1981). *Biology of Insect Eggs*. Oxford; New York: Pergamon Press.

Huang, J., Zhou, W., Dong, W., Watson, A. M. and Hong, Y. (2009). Directed, efficient, and versatile modifications of the Drosophila genome by genomic engineering. *Proc. Natl. Acad. Sci. USA* **106**, 8284-8289.

James, K. E. and Berg, C. A. (2003). Temporal comparison of Broad-Complex expression during eggshell-appendage patterning and morphogenesis in two Drosophila species with different eggshell-appendage numbers. *Gene Expr. Patterns* **3**, 629-634.

Kagesawa, T., Nakamura, Y., Nishikawa, M., Akiyama, Y., Kajiwara, M. and Matsuno, K. (2008). Distinct activation patterns of EGF receptor signaling in the homoplastic evolution of eggshell morphology in genus Drosophila. *Mech. Dev.* **125**, 1020-1032.

Mallarino, R. and Abzhanov, A. (2012). Paths less traveled: evo-devo approaches to investigating animal morphological evolution. *Annu. Rev. Cell Dev. Biol.* **28**, 743-763.

Mallarino, R., Campàs, O., Fritz, J. A., Burns, K. J., Weeks, O. G., Brenner, M. P. and Abzhanov, A. (2012). Closely related bird species demonstrate flexibility between beak morphology and underlying developmental programs. *Proc. Natl. Acad. Sci. USA* **109**, 16222-16227.

Marmion, R. A., Jevtic, M., Springhorn, A., Pyrowolakis, G. and Yakoby, N. (2013). The Drosophila BMPRII, wishful thinking, is required for eggshell patterning. *Dev. Biol.* **375**, 45-53.

Meijering, E., Jacob, M., Sarria, J.-C. F., Steiner, P., Hirling, H. and Unser, M. (2004). Design and validation of a tool for neurite tracing and analysis in fluorescence microscopy images. *Cytometry* **58A**, 167-176.

Nakamura, Y. and Matsuno, K. (2003). Species-specific activation of EGF receptor signaling underlies evolutionary diversity in the dorsal appendage number of the genus Drosophila eggshells. *Mech. Dev.* **120**, 897-907.

Nakamura, Y., Kagesawa, T., Nishikawa, M., Hayashi, Y., Kobayashi, S., Niimi, T. and Matsuno, K. (2007). Soma-dependent modulations contribute to divergence of rhomboid expression during evolution of Drosophila eggshell morphology. *Development* **134**, 1529-1537.

Niepielko, M. G. and Yakoby, N. (2014). Evolutionary changes in TGFalpha distribution underlie morphological diversity in eggshells from Drosophila species. *Development* **141**, 4710-4715.

Niepielko, M. G., Hernáiz-Hernández, Y. and Yakoby, N. (2011). BMP signaling dynamics in the follicle cells of multiple Drosophila species. *Dev. Biol.* **354**, 151-159.

Niepielko, M. G., Ip, K., Kanodia, J. S., Lun, D. S. and Yakoby, N. (2012). Evolution of BMP signaling in Drosophila oogenesis: a receptor-based mechanism. *Biophys. J.* **102**, 1722-1730.

Niepielko, M. G., Marmion, R. A., Kim, K., Luor, D., Ray, C. and Yakoby, N. (2014). Chorion patterning: a window into gene regulation and Drosophila species' relatedness. *Mol. Biol. Evol.* **31**, 154-164.

Osterfield, M., Du, X., Schüpbach, T., Wieschaus, E. and Shvartsman, S. Y. (2013). Three-dimensional epithelial morphogenesis in the developing Drosophila egg. *Dev. Cell* **24**, 400-410.

Peri, F., Bökel, C. and Roth, S. (1999). Local Gurken signaling and dynamic MAPK activation during Drosophila oogenesis. *Mech. Dev.* **81**, 75-88.

Peters, N. C., Thayer, N. H., Kerr, S. A., Tompa, M. and Berg, C. A. (2013). Following the 'tracks': Tramtrack69 regulates epithelial tube expansion in the Drosophila ovary through Paxillin, Dynamin, and the homeobox protein Mirror. *Dev. Biol.* **378**, 154-169.

Russo, C. A., Takezaki, N. and Nei, M. (1995). Molecular phylogeny and divergence times of drosophilid species. *Mol. Biol. Evol.* **12**, 391-404.

Suzuki, A. and Ohno, S. (2006). The PAR-aPKC system: lessons in polarity. *J. Cell Sci.* **119**, 979-987.

Vreede, B. M. I., Lynch, J. A., Roth, S. and Sucena, E. (2013). Co-option of a coordinate system defined by the EGFr and Dpp pathways in the evolution of a morphological novelty. *Evodevo* **4**, 7.

Ward, E. J. and Berg, C. A. (2005). Juxtaposition between two cell types is necessary for dorsal appendage tube formation. *Mech. Dev.* **122**, 241-255.

Wu, X., Tanwar, P. S. and Raftery, L. A. (2008). Drosophila follicle cells: morphogenesis in an eggshell. *Semin. Cell Dev. Biol.* **19**, 271-282.

Yamada, T., Okabe, M. and Hiromi, Y. (2003). EDL/MAE regulates EGF-mediated induction by antagonizing Ets transcription factor Pointed. *Development* **130**, 4085-4096.

Zallen, J. A. and Wieschaus, E. (2004). Patterned gene expression directs bipolar planar polarity in Drosophila. *Dev. Cell* **6**, 343-355.

Zartman, J. J., Yakoby, N., Bristow, C. A., Zhou, X., Schlichting, K., Dahmann, C. and Shvartsman, S. Y. (2008). Cad74A is regulated by BR and is required for robust dorsal appendage formation in Drosophila oogenesis. *Dev. Biol.* **322**, 289-301.

Zartman, J. J., Cheung, L. S., Niepielko, M. G., Bonini, C., Haley, B., Yakoby, N. and Shvartsman, S. Y. (2011). Pattern formation by a moving morphogen source. *Phys. Biol.* **8**, 045003.

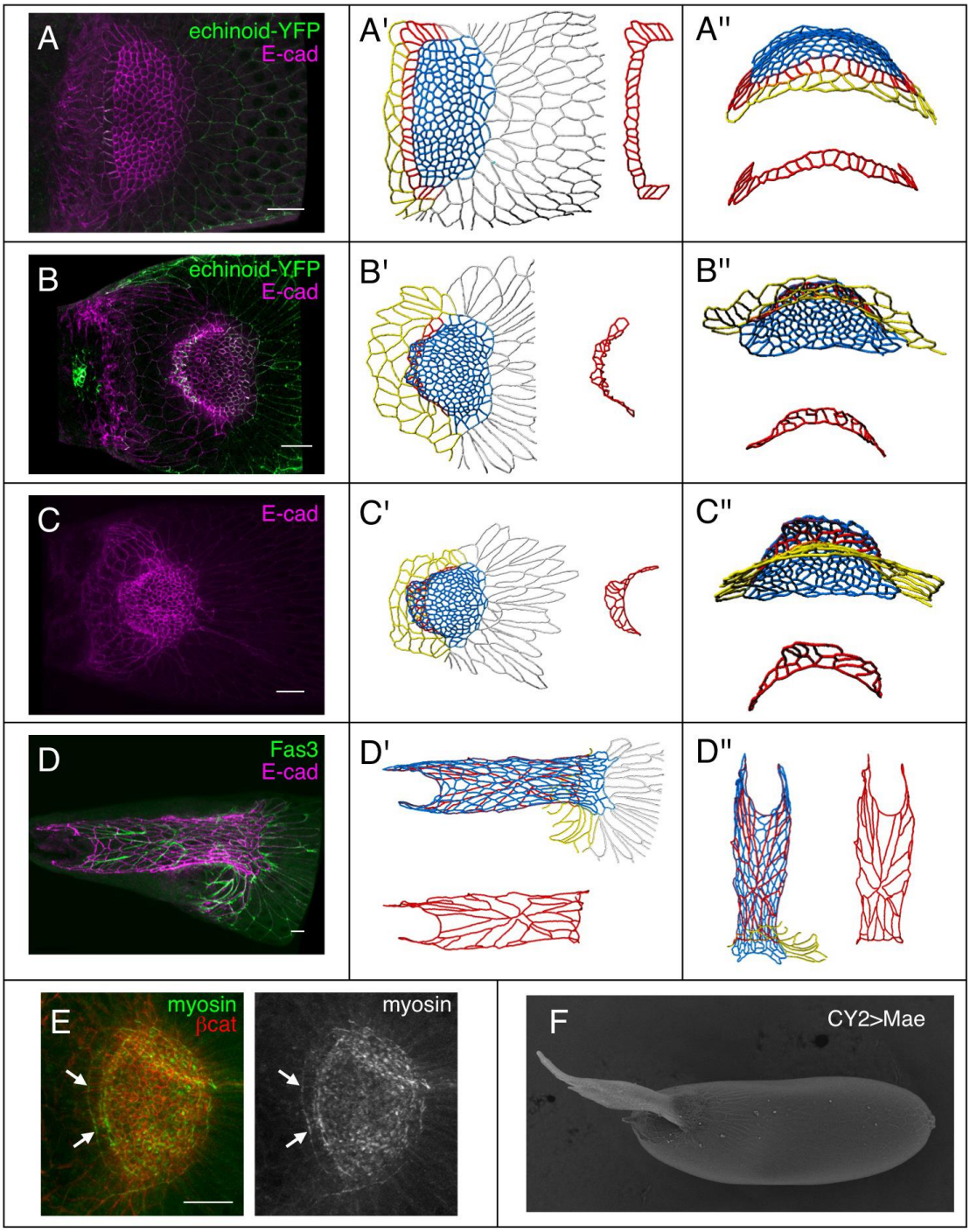

Figure S1: Dorsal appendage formation in *D. melanogaster* patterning mutant CY2>Mae.

(A-D) Immunostainings of CY2>Mae egg chambers for apical marker E-cadherin (magenta). Additional staining for echinoid-YFP or Fas3 was carried out to assist in

identifying specific cell types and in particular to help with visualizing the floor cells. Anterior is left. All scale bars = 20 microns.

(A'-D") 3D reconstructions of data from (A-D). Putative cell types were assigned according to cell morphology and color-coded as follows: blue, roof; red, floor; yellow, 'midline' or operculum-forming cells; and gray, main body cells. Views shown in (A'-D') are approximately dorsal. Views chosen to optimize visualization of the floor cells (roughly from the anterior) are shown in (A"-D").

(E) Immunostaining of CY2>Mae egg chambers for β-catenin (red) and phospho-myosin regulatory light chain (green). Image was cropped to remove basal surface and reveal underlying apical surface. Myosin cable along the floor-midline boundary is indicated with arrows. Dorsal view, anterior is left, scale bar = 20 microns.

(F) SEM image of CY2>GAL4 eggshell, showing a single, wide appendage.

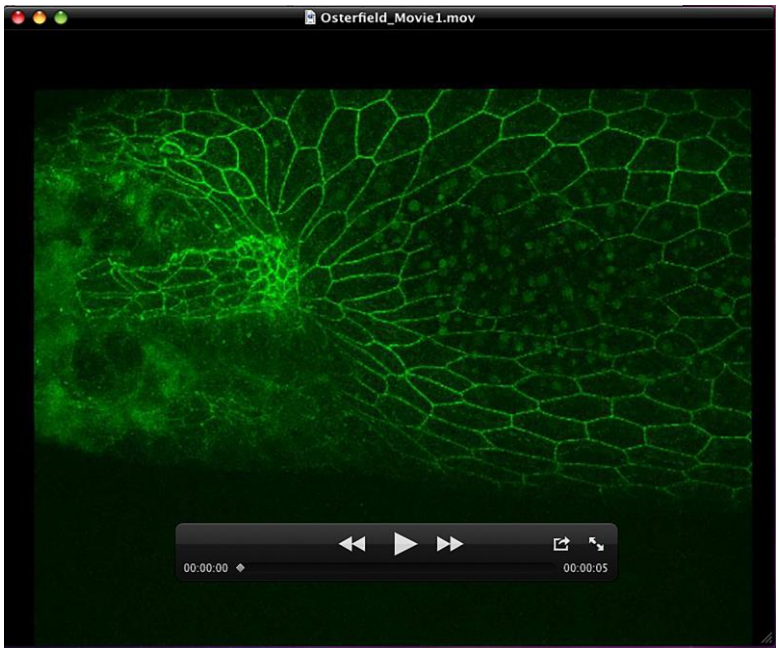

Movie 1: 3D reconstructions of dorsal appendage formation in *D. melanogaster*. The image shown rotating here is from Figure 1C, the 135 minute time point. The apical outlines of follicle cells, visualized with E-cadherin:GFP, are shown first in green. The filament tracing, shown next, is color-coded as in Figure 1; specifically, blue = roof; red = floor; yellow = “midline”, or operculum-forming cells; and gray = main body cells.

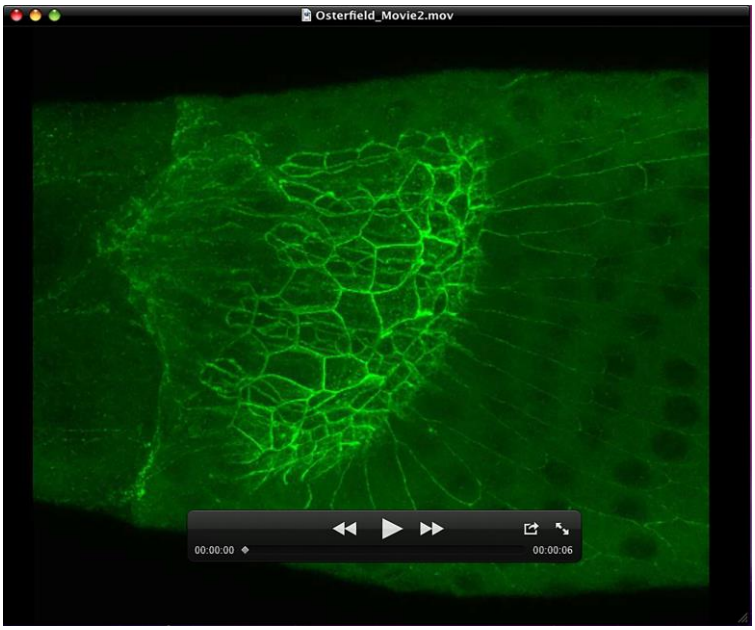

Movie 2: 3D reconstructions of dorsal appendage formation in *S. pattersoni*. The image shown rotating here is from Figure 2D-D'. The apical outlines of follicle cells, visualized with β-catenin antibody staining, are shown first in green. The filament tracing, shown next, is color-coded as in Movie 1. The floor tracing (red) alone is shown for the final frame.

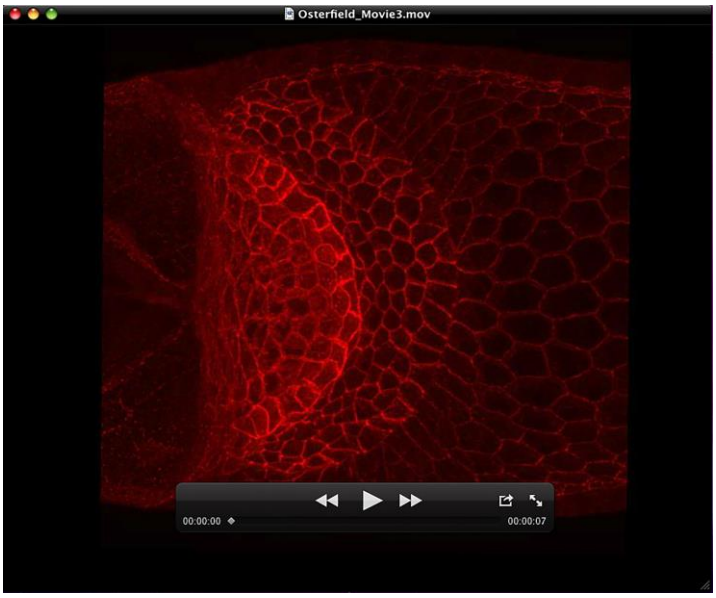

Movie 3: Bazooka and aPKC co-localize to the elongating set of floor-floor edges in *S. pattersoni*. Immunostaining of *S. pattersoni* egg chambers for β-catenin (red) is shown first to show overall tissue morphology, then Bazooka (cyan), and aPKC (green) are added. The image shown rotating here, uncropped, is from the same sample as Figure 3G, right panel.

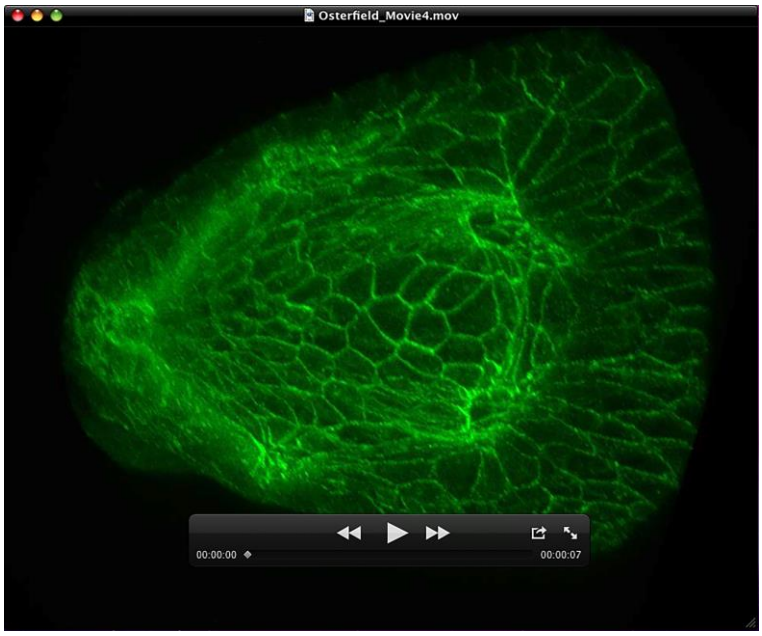

Movie 4: 3D reconstructions of dorsal appendage formation in *D. funebris*. The image shown rotating here is from Figure 4H-H'. The apical outlines of follicle cells, visualized with β-catenin antibody staining, are shown first in green. A filament tracing encompassing both lower (i.e. left) appendages is shown next in gray. The posterior of these appendages is then color-coded as in Movie 1. The floor tracing (red) alone is shown for the final frame.